Effect Analysis of Wearing an Lumbar Exoskeleton on Coordinated Activities of the Low Back Muscles Using sEMG Topographic Maps

Naifu Jiang, *Member, IEEE*, Dashuai Wang, Xinyu Ji, Lin Wang, *Member, IEEE*, Xinyu Wu, *Senior Member, IEEE*, and Guanglin Li, *Senior Member, IEEE*

***Abstract*— Lumbar exoskeleton has potential to assist in lumbar movements and thereby prevent impairment of back muscles. However, due to limitations of evaluation tools, the effect of lumbar exoskeletons on coordinated activities of back muscles is seldom investigated. This study used the surface electromyography (sEMG) topographic map based on multi-channel electrodes from low back muscles to analyze the effects. Thirteen subjects conducted two tasks, namely lifting and holding a 20kg-weight box. For each task, three different trials, not wearing exoskeleton (NoExo), wearing exoskeleton but power-off (OffExo), and wearing exoskeleton and power-on (OnExo), were randomly conducted. Root-mean-square (RMS) and median-frequency (MDF) topographic maps of the recorded sEMG were constructed. Three parameters, average pixel values, distribution of center of gravity (CoG), and entropy, were extracted from the maps to assess the muscle coordinated activities. In the lifting task, results showed the average pixel values of RMS maps for the NoExo trial were lower than those for the OffExo trial ($p<0.05$) but the same as those for the OnExo trial ($p>0.05$). The distribution of CoG showed a significant difference between NoExo and OnExo trials ($p<0.05$). In the holding task, RMS and MDF maps' average pixel values showed significant differences between NoExo and OnExo trials ($p<0.05$). These findings suggest that active lumbar exoskeletons can reduce the load on low back muscles in the static holding task rather than in the dynamic lifting task. This proves sEMG topographic maps offer a new way to evaluate such effects, thereby helping improve the design of lumbar exoskeleton systems.**

***Index Terms*— Electromyography, brain–computer interface, human-computer interface, low back pain, muscle coordination.**

Manuscript received 12 October 2023; revised 12 December 2023; accepted 29 December 2023. Date of publication 2 January 2024; date of current version 16 January 2024. This work was supported in part by the National Natural Science Foundation of China under Grant 62001463 and Grant 81927804, in part by the Guangdong Basic and Applied Basic Research Foundation under Grant 2021A1515011918, and in part by the Shenzhen Science and Technology Program under Grant JCYJ20210324102010029 and Grant KQTD20210811090217009. *(Naifu Jiang and Dashuai Wang contributed equally to this work.) (Corresponding authors: Xinyu Wu; Guanglin Li.)*

This work involved human subjects or animals in its research. Approval of all ethical and experimental procedures and protocols was granted by the Institutional Review Board of Shenzhen Institute of Advanced Technology, Chinese Academy of Sciences under IRB No. SIAT-IRB-200715-H0512, July 2020.

Naifu Jiang, Lin Wang, Xinyu Wu, and Guanglin Li are with the CAS Key Laboratory of Human-Machine Intelligence-Synergy Systems, the Shenzhen Institute of Advanced Technology (SIAT), the Chinese Academy of Sciences (CAS), and the SIAT Branch, Shenzhen Institute of Artificial Intelligence and Robotics for Society, Shenzhen 518055, China, and also with the Guangdong-Hong Kong-Macao Joint Laboratory of Human-Machine Intelligence-Synergy Systems, Shenzhen 518055, China (e-mail: nf.jiang@siat.ac.cn; lin.wang1@siat.ac.cn; xy.wu@siat.ac.cn; gl.li@siat.ac.cn).

Dashuai Wang is with the School of Microelectronics, Southern University of Science and Technology, Shenzhen 518055, China (e-mail: wangds3@sustech.edu.cn).

Xinyu Ji is with CETHIK Group Company Ltd., Hangzhou 310000, China (e-mail: shea115@163.com).

Digital Object Identifier 10.1109/TNSRE.2023.3349189

I. Introduction

LOW back muscles are significant to support human bodies [1]. Long-term and high-intensity lumbar movement (e.g., cargo handling, patient handling) can lead to a high risk of disorder of low back muscles (e.g., low back pain), which will severely interfere with people's work efficiency and life quality [2]. In recent years, lumbar exoskeleton (LEXO) is developed to assist in lumbar movement. It showed potential to relieve muscle fatigue and improve work efficiency by reducing the workload for low back muscles [3], [4], [5].

In order to accurately evaluate the effect of lumbar exoskeleton on low back muscles and improve the exoskeleton system, activities of low back muscles were often measured and analyzed. The researchers generally recorded surface electromyography (sEMG) from low back muscles to view the muscle activities [3], [4], [5], [6], [7], [8]. After wearing a passive lumbar exoskeleton, there showed a significant reduction in the root mean square (RMS), zero-crossing rate, mean frequency, median frequency of sEMG from some paraspinal muscles during lifting movement [6]. The active exoskeleton could significantly reduce the back muscular activity during repetitive lifting tasks [7], [8]. It was shown with a reduction of average integrated sEMG and amplitude of sEMG for lumbar

muscles. The lumbar exoskeleton also showed a potential use to help farmers work under less muscular load, by decreasing back muscular activity during farm tasks [9]. Although there are many studies using sEMG to explore the effect of lumbar exoskeleton on low back muscles, most of them only placed emphasis on the measurement of activities of single muscles rather than the coordinated activity of muscle groups, which resulted in an incomprehensive and inaccurate evaluation of the effect of exoskeleton on low back muscles.

There are mainly two ways to investigate the effect of the lumbar exoskeleton on the coordination/synergy of low back muscles. The non-negative matrix factorization (NMF) algorithm [10], which was commonly applied in the analysis of muscle synergy for the lower-limb exoskeleton [11], was used to compute the muscle synergies from different muscles. By collecting the sEMG data from several superficial muscles (biceps brachii, latissimus dorsi, erector spinae, gluteus maximus) and comparing the muscle coordination patterns during fatigue task, it was found the timing coefficients of the synergies (synergy weights) significantly changed after wearing a lumbar exoskeleton [10]. However, this kind of synergy analysis method is sensitive to methodological choices and experimental conditions [12], [13], which can lead to an inaccurate and unstable conclusion. sEMG topographic map is another tool to assess muscle synergy. It is produced based on the multi-channel array's sEMG signals. Compared with the traditional single-channel bipolar recording method, this multi-channel monopolar recording method can provide information on the spatial distribution of electric potentials over the skin surface during muscle contraction [14]. By using two small electrode grids beside the spine, the sEMG topographic map was obtained to assess the effectiveness of a passive lumbar exoskeleton [15]. The average RMS amplitude decreased and the distribution of muscle activity in the map changed during tasks. This study initially showed the potential use of the sEMG topographic map for the evaluation of the lumbar exoskeleton. Nonetheless, it only analyzed the muscles and part of a muscle beside the spine, ignoring other muscles located in the entire low back region. Hence, a global sEMG topographic map covering all low-back regions is required.

High-density surface electromyography (HD-sEMG) is a technique that involves the concurrent recording of at least 4 sEMG signals with closely spaced (normally 2.5-10 mm), small-diameter (0.5-3 mm) electrodes [16]. In contrast to HD-sEMG, the multi-channel array's sEMG technique has no requirement on the inter-electrode distance and the electrode size. In evaluating the impact of the lumbar exoskeleton, the use of the multi-channel array's sEMG technique is preferable to the HD-sEMG for constructing the sEMG topographic map, and this is attributed to the following reasons: Firstly, due to individual variations and the considerable size of the lumbar region, maintaining consistent anatomical positioning beneath each surface EMG electrode becomes challenging when the inter-electrode distance is kept constant, especially across different individuals [17]. This inconsistency would impede the meaningful comparison of sEMG topographic maps among individuals. Consequently, a more appropriate approach involves evenly placing all surface EMG electrodes on the skin in the low back region. The use of some HD-sEMG sensors, which were integral multi-channel electrode array patches with a fixed inter-electrode distance, was not suitable for this study. Secondly, the size of HD-sEMG electrodes may not yield satisfactory signal quality when subjects wear a lumbar exoskeleton. Various factors affect sEMG signal quality during experiments, with one major factor being the pressure exerted by the lumbar exoskeleton. Since the electrodes are positioned between the exoskeleton and the skin of the low back region, the exoskeleton's body can repeatedly come into contact with and press against the electrodes during lifting-drop experiments. If the electrode size is too small, it may easily dislodge under these conditions.

In addition, there are mainly two types of movement modes in the process of moving objects: lifting mode and holding mode. They require different ways of muscle contraction: dynamic (or isotonic) contraction and static (or isometric) contraction [18]. Dynamic contraction generates force by changing the length of the muscle, whereas static contraction generates force without changing the length of the muscle. The patterns of motor unit activation within the muscles are different for these two types of muscle contractions, which reflect the characteristics of muscles (strength, endurance, et. al.) [19]. In high-intensity physical work, both dynamic and static lumbar movements are required [20]. It is significant to explore how the lumbar exoskeleton affects the coordinated activities of muscles under different types of muscle contractions.

Therefore, current work cannot accurately reveal the alteration of the synergy pattern of all relevant low back muscles when wearing a lumbar exoskeleton. By using the global sEMG topographic map computed from multi-channel electrode arrays' signals, this study aimed to evaluate the effect of the lumbar exoskeleton on coordinated activities of low back muscles in the lifting mode and holding mode. It will help to improve the design of lumbar exoskeleton systems.

II. Exoskeleton Description

The lumbar exoskeleton used in this study is produced in our lab (Fig. 1). It is an active lumbar exoskeleton (weight: 4.9kg) which can provide assistance and protection for the wearer's lumbar vertebrae joints during lumber movement [3]. The lumbar exoskeleton is composed of the following three sub-modules: (a) physical human-robot interface, (b) principle of assistance, and (c) control strategy.

A. Physical Human-Robot Interface

In order to ergonomically fit the wearer's lumbar spine, the lumbar exoskeleton was comprised of an inverted-T-shaped frame shell, a set of adjustable fastening belts (shoulder belt, chest belt, pelvis belt, and thigh belt), as well as two thigh braces (Fig. 1a). In the frame shell, we embedded a lithium battery (48.1 V, 2000 mAh), a microcontroller-unit-based control system, and two hip actuators to activate the exoskeleton. Each hip actuator (peak torque: 42 N.m) integrated an ODrive motor controller, a brushless motor with harmonic drive (gear ratio: 6:1), and a 14-bit on-axis rotary position

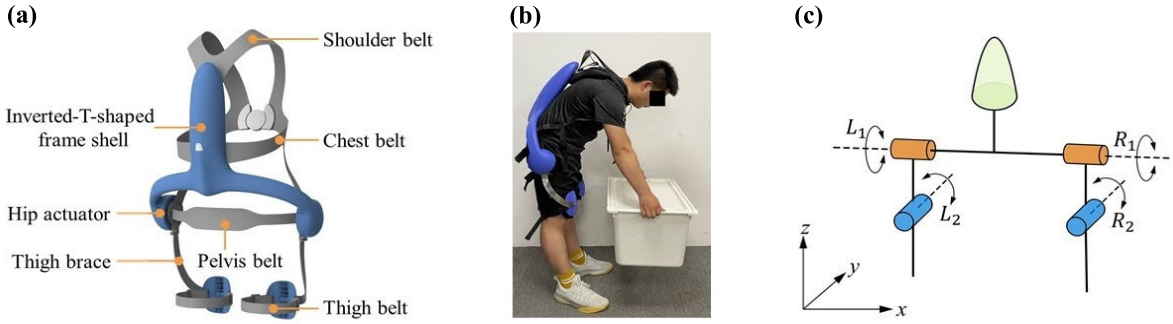

Fig. 1. Design of lumbar exoskeleton (LEXO). (a) Structural framework of LEXO. (b) Subject wearing LEXO while performing a lifting movement. (c) DOFs chain of LEXO.

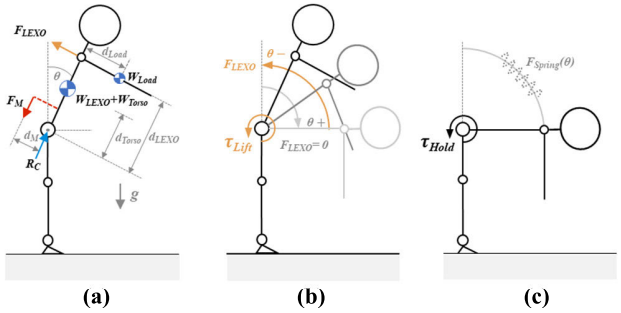

Fig. 2. Biomechanical model of lumbar exoskeleton (LEXO). (a) Kinetics analysis of simplified Human-LEXO model. (b) Lifting-assistive mode. (c) Holding-assistive mode.

magnetic encoder (AS5047P). The thigh brace bridged the tunnel between the hip joints and the wearer's thigh to transmit the assistive torque. By adjusting the fastening belts, the lumbar exoskeleton was suitable for the wearer with a height ranging from 160 to 185 cm. Fig. 1b shows the subject wearing the lumbar exoskeleton while performing a lifting movement.

Fig. 1c depicts four DOFs (degree of freedom) chain of the lumbar exoskeleton. The DOFs chain on each side includes two rotational degrees. One is the active rotational degree (L1/R1) and the other is the passive rotational degree (L2/R2). The active rotational degree is aligned with the hip flexion/extension rotation in the sagittal plane, while the passive rotational degree is in line with the hip abduction/adduction movement in the coronal plane. L1/R1 is produced by an actuator generating the active assistive torque, when L2/R2 is produced depending on the hip abduction/adduction without external resistance.

B. Biomechanical Model of Lumbar Exoskeleton

Fig.2a demonstrates the kinetics analysis of biomechanical model of Human-LEXO on the two-dimensional sagittal plane. The torso of the human body and the upper part of lumbar exoskeleton were regarded as a main rigid body. In order to simplify the kinetic model, we supposed the moment of inertias of human torso, lumbar exoskeleton and external load were applied to their centers of mass ignoring the mass and movement of human arms.

According to previous study [21], we used F_M to represent the force generated by lumbar muscles to balance the motion of human torso, unpowered lumbar exoskeleton, and lifted load. The reaction force R_C at the joint captured the lumbar compressive loads, which the exoskeleton aimed to reduce. They can be calculated via the following dynamic equilibriums:

$$\begin{aligned} F_M d_M = {} & g\left(W_{LEXO} + W_{Torso}\right) d_{Torso} \sin\theta \\ & + g W_{Load}\left(d_{LEXO}\sin\theta + d_{Load}\cos\theta\right) \\ & - \left(J_{LEXO} + J_{Torso} + J_{Load}\right)\ddot{\theta} \\ & - d_{Load} d_{LEXO}\dot{\theta}^2 W_{Load} \end{aligned} \tag{1}$$

$$\begin{aligned} R_C = {} & F_M + g\left(W_{LEXO} + W_{Torso} + W_{Load}\right)\cos\theta \\ & - d_{Torso}\dot{\theta}^2\left(W_{LEXO} + W_{Torso}\right) - d_{LEXO}\dot{\theta}^2 W_{Load} \end{aligned} \tag{2}$$

where g is the gravity; θ is the angle between the torso and the direction of gravity, whose value is zero corresponding to straight standing and positive corresponding to forward bending; $\dot{\theta}$ and $\ddot{\theta}$ denote the derived angular velocity and angular acceleration respectively; W_{Torso}, W_{LEXO}, and W_{Load} indicate the masses of the human torso, the upper part of the lumbar exoskeleton and the external load respectively; J_{Torso}, J_{LEXO}, and J_{Load} are the moment of inertias of the human torso, the upper part of lumbar exoskeleton and the external load;d_M is the vertical distance between the human torso and the line of lumbar muscles, and it was set as 5cm in this study [21]; d_{Torso} and d_{LEXO} are the distances from the center of mass in human torso and in shoulder joint to the rotation axis of lumbar exoskeleton hip actuator respectively; d_{Load} represents a constant distance between the center of mass of external load and center of mass in human shoulder joint.

Lumbar exoskeleton works by transferring the load from the lumbar spine to other endurable body parts, so that the activation of lumbar muscles reduces and the compression on lumbar facet joints alleviates. According to experimental design, we proposed two assistive modes for lumbar exoskeleton, namely lifting-assistive mode (Fig. 2b) and holding-assistive mode (Fig. 2c). In lifting-assistive mode, the lumbar exoskeleton provided active assistance with lifting up (θ-) and maintained in a free state with lifting down (θ+). In holding-assistive mode, the lumbar exoskeleton was

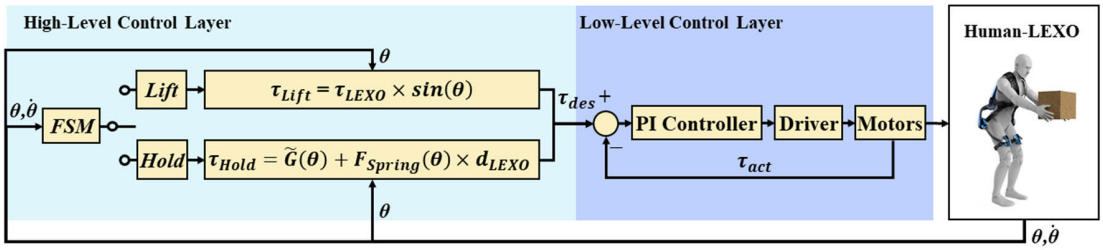

Fig. 3. Control strategy of lumbar exoskeleton (LEXO).

designed to help wearer carry a heavy load with a constant bending angle maintaining by providing a static assistive vector. After lumbar exoskeleton works, it can generate a force (F_{LEXO}) which is perpendicular to the torso around the wearer's shoulder joint. F_M^{LEXO} and R_C^{LEXO} are defined to indicate the F_M and R_C respectively with F_{LEXO} and they should be decrease as much as possible. F_M^{LEXO} and R_C^{LEXO} can be calculated by the following dynamic equilibriums:

$$F_M^{LEXO} = F_M - F_{LEXO}\frac{d_{LEXO}}{d_M} \tag{3}$$

$$R_C^{LEXO} = F_M^{LEXO} + g\left(W_{LEXO} + W_{Torso} + W_{Load}\right)\cos\theta - d_{Torso}\dot{\theta}^2\left(W_{LEXO} + W_{Torso}\right) - d_{LEXO}\dot{\theta}^2 W_{Load} \tag{4}$$

C. Control Strategy

The lumbar exoskeleton control strategy is deployed with a two-layer architecture (Fig. 3), including a High-Level Control Layer (HLCL), running on a real-time microcontroller unit (MCU) embedded system, and a Low-Level Control Layer (LLCL), performed by the motor driver. With the feedback data from encoder sensors, the HLCL can recognize the wearer's movement mode (lifting-assistive mode or holding-assistive mode) via a finite state machine (FSM). In the lifting-assistive mode, active assistive torque τ_{Lift} is generated by the HLCL through the torque control method, while in the holding-assistive mode, τ_{Hold} is produced through the position control method. Then in the LLCL, the motor driver receives the target assistive torque (τ_{des}) from HLCL and controls the hip actuator via a closed-loop PI torque controller.

In the lifting-assistive mode, in order to dynamically adjust the assistive torque (τ_{Lift}) according to changes in bending angle θ, each hip actuator is controlled to generate the Sine torque [22].

$$\tau_{Lift} = \tau_{LEXO} \times sin\theta \tag{5}$$

where τ_{LEXO} is the maximum output torque of hip actuator. In a special case, at initial straight standing position (θ =0), the lumbar exoskeleton would work in a free mode to avoid causing any discomfort.

In the holding-assistive mode, both gravity compensation for the upper part of lumbar exoskeleton ($\tilde{G}(\theta)$) and the virtual spring force ($F_{Spring}(\theta)$) [23] are considered in the calculation of static assistive torque of τ_{Hold}.

$$\tau_{Hold} = \tilde{G}(\theta) + F_{Spring}(\theta) \times d_{LEXO} \tag{6}$$

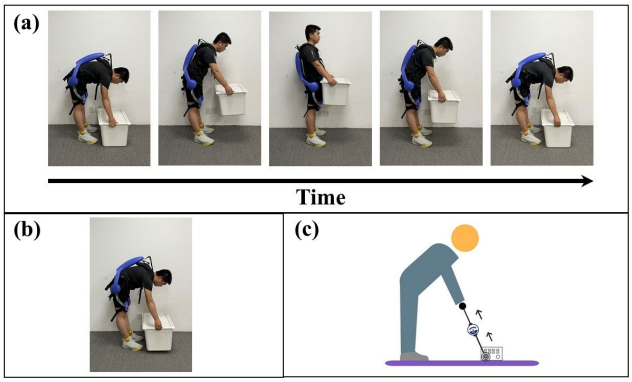

Fig. 4. Design of experimental tasks. (a) Lifting task with a cycle of lift-drop movement; (b) Holding task with a holding posture; (c) Measurement of the sEMG data under maximum voluntary contraction.

Additionally, τ_{LEXO} and $F_{Spring}(\theta)$ are configurable to match individual preferences and task requirements.

III. Experimental Evaluation

A. Experimental Design

As shown in Fig. 4, subjects were asked to perform 2 tasks (lifting task and holding task). In the lifting task, subjects were asked to lift and drop a 20kg of box (Fig. 4a). They performed the lift-drop movement 5 times/cycles within one minute at a consistent speed. In the holding task, subjects were asked to lift a 20kg of box and maintain the holding posture until the severe involuntary body-shaking appeared. The holding posture was displayed in Fig. 4b, in order to make the low back muscles play the primary role in the holding procedure. Besides, for each task, each subject participated in three different trials: not wearing an exoskeleton (NoExo), wearing an exoskeleton but power-off (OffExo), and wearing an exoskeleton and power-on (OnExo). A plenty-time break was given to subjects between trials to ensure no fatigue was reported by the participant. The sEMG data were collected in all trials of two tasks, while the assessment data for fatigue-related characteristics (maintaining duration of holding posture) was recorded only in trials of the holding task. In order to avoid bias, the assignment of both tasks (lifting task, holding task) and exoskeleton conditions (NoExo trial, OffExo trial, OnExo trial) was randomized for each subject using computer-generated random numbers. The random number was placed in a sealed and opaque envelope and implemented by the independent researcher. Subsequently, the experimental sequence (representing one

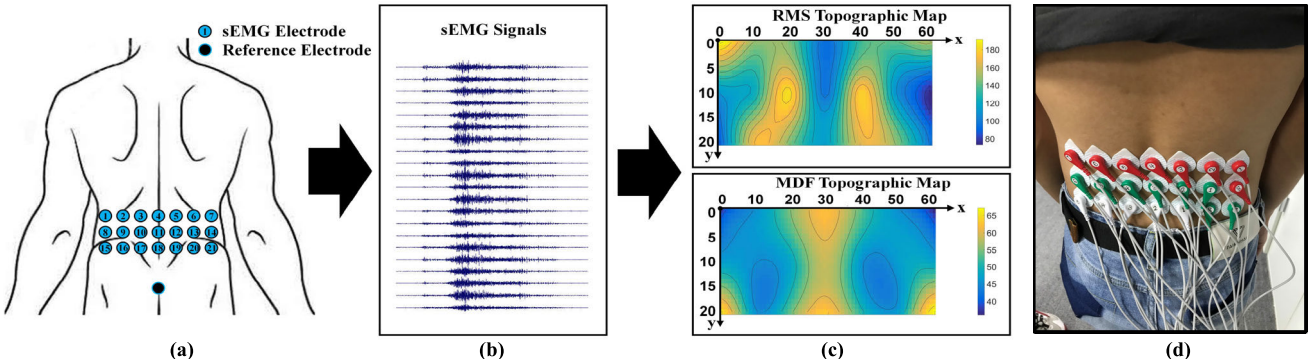

Fig. 5. sEMG measurement and analysis. (a) Placement of sEMG electrodes. (b) Multi-channel sEMG signals. (c) sEMG topographic maps with the vertical (no uint) and horizontal axes (unit: pixel). (d) sEMG Electrodes.

exoskeleton condition in one task) for each subject was organized in accordance with the generated random numbers. Before the experiment, each subject was asked to pull a back dynamometer with a maximal lumbar force, so that the sEMG data under maximum voluntary contraction (MVC) could be recorded. In alignment with the previous study [24], the subject was asked to pull the back dynamometer with a maximal lumbar force, keeping their legs and trunk straight, only the upper limb that pulled as demonstrated in the Fig. 4c. This pulling position was to be sustained for 15 seconds, during which the sEMG data was recorded. The subject performed this task twice, separated by a 5-minute rest period between tasks. The average sEMG data from these two tasks was then calculated to represent the maximum voluntary contraction (MVC) data.

B. Participants

A total of thirteen healthy male participants were recruited from the Shenzhen Institutes of Advanced Technology, Chinese Academy of Sciences. The demographic characteristics were shown in Table I. When recruiting subjects, we used the 11-point numeric rating scale (NRS) for pain to assess the intensity of low back pain (LBP) [25]. For inclusion in this study, only subjects with an NRS score of zero for LBP were eligible for recruitment. We excluded individuals who had a history of psychiatric, neurological, implanted medical devices, or currently taking psychotropic medications. Participants' characteristics including physiological and psychological variables were recorded before the experiment. All participants gave their written informed consent before testing and were paid for their participation. The experimental procedure was performed in accordance with the Declaration of Helsinki and was approved by the Institutional Review Board of Shenzhen Institute of Advanced Technology, Chinese Academy of Sciences (IRB No.: SIAT-IRB-200715-H0512, July 2020).

C. Fatigue-Related Characteristics Assessment

Maintaining duration of holding posture was recorded in the holding task. The maintaining duration (unit: seconds) was defined as the duration from the beginning time of the holding posture to the time when the involuntary body-shaking can be observed obviously. We used the "involuntary body-shaking" as the endpoint, because it indicated the limit state of muscle fatigue was reached. Generally, when muscle fatigue level is above a threshold, the muscle spasm will appear [26]. It can cause the appearance of involuntary body-shaking, which can be obviously observed. If the holding task was still performed, the muscles injury might appear. Hence, the "involuntary body-shaking" can be an appropriate objective criterion for all subjects to finish the fatiguing trial.

TABLE I
PARTICIPANT CHARACTERISTICS

Characteristics	Mean ± Standard Deviation
Age (years)	24.9 ± 2.2
Weight (kg)	64.7 ± 5.9
Height (cm)	173.9 ± 5.3
BMI (kg/m^2)	21.4 ± 1.6

BMI = Body Mass Index.

D. sEMG Measurement

The surface electrodes (Ag/AgCl electrode) in a 3×7 array (21 electrodes) were evenly attached to the skin in the low back area between the lateral edges of the torso (horizontally) and the L2-L4 level (vertically). Another electrode was attached to the surface of the sacral vertebrae as the ground electrode (GND). In order to make the placement of the electrodes understood more easily, the detailed location of electrodes was also shown in Fig. 5a. Our preliminary experiment indicated that the commonly used electrodes with a diameter of 1.5 cm are suitable for this study. These electrodes securely adhered to the skin of the low back region, and the exoskeleton's pressure had minimal impact on the quality of the EMG signal. Before the sEMG electrodes were attached, the skin preparation for sEMG was done according to the following procedures to keep the skin impedance less than 10 kΩ: cleaning the site with alcohol, shaving the electrode site (if the skin surface at the sensor location was covered with noticeable hair), and lightly abrading the skin with fine sandpaper. The monopolar sEMG signals from the 21 sEMG electrodes were differentially amplified versus the reference electrode (Fig. 5b). The sEMG

signal was acquired at a sample rate of 1024 Hz and was band-filtered between 10 and 500 Hz (REFA, TMSi International, the Netherlands). 50Hz powerline influence was removed by digital notch filters. The cardiac artifact was filtered by the independent component analysis (ICA) method.

E. Data Analysis

After 21 channels of sEMG signals were preprocessed, the time-domain and frequency-domain features were extracted. The root-mean-square (RMS) was used as the time-domain feature, while the median frequency (MDF) was selected as the frequency-domain feature [27]. The calculation of features was different between sEMG data in the lifting task and holding task. In the lifting task, sEMG data in the five cycles of lift-drop movements were respectively extracted to compute the RMS and MDF features. These features were then averaged to reach the final features. Besides, in order to evaluate the situation-specific effects of the exoskeleton, the sEMG data in the lifting task should be respectively analyzed in the lifting-up phase, the holding phase, and the lifting-down phase. However, owing to the shaking body during the holding phase, it was difficult to measure the low back muscle activity in the holding phase. Consequently, only the sEMG data in the lifting-up phase and lifting-down phase were analyzed. The muscle activities in the holding phase were assessed in the holding task. In the holding task, the data was equally divided into three time phases ('First Phase', 'Second Phase', 'Third Phase'). RMS and MDF features in each phase were obtained. All RMS features were normalized to the RMS value from MVC. By using the method of linear cubic spline interpolation [28], [29], the feature space among electrodes was filled to construct the sEMG topographic map (RMS topographic map and MDF topographic map) with a 20×60 coordinate system in Fig 5c. In our earlier investigations involving patients with low back pain [28], [29], the electrode placement and size employed in this study were effectively utilized to create the sEMG topographic map. The accuracy of assessing the activities of the low back muscles through the sEMG topographic map has been validated.

For a visual comparison of differences among sEMG topographic maps, we attempted to normalize the maps across various conditions (NoExo trial, OffExo trial, OnExo trial) and different phases (lifting task: lifting-up phase vs. lifting-down phase; holding task: First Phase vs. Second Phase vs. Third Phase). The maximum pixel value across all maps, considering different conditions and phases, served as the upper threshold for map normalization, while the minimum pixel value established the lower threshold. Subsequently, all maps underwent normalization using these threshold values. Although the normalized results still varied among subjects and tasks (lifting task, holding task), we preemptively normalized the original sEMG signal using the sEMG data during MVC to avoid biases arising from subjects and tasks.

In order to characterize the spatial distribution of muscle activity, four different types of variables were extracted from sEMG topographic map: average pixel value over the entire sEMG topographic map (RMS_Mean, MDF_Mean), the coordinate of the center of gravity (CoG) of sEMG topographic map in the horizontal direction (RMS_CoGx, MDF_CoGx) and vertical direction (RMS_CoGy, MDF_CoGy) [30], the entropy of sEMG topographic map (RMS_Entropy, MDF_Entropy). The coordinates in the sEMG topographic map for the calculation of CoG were displayed in Fig. 5c. The unit of the coordinate was defined corresponding to the position of electrodes.

The parameters of Mean (RMS_Mean and MDF_Mean), CoG (CoGx and CoGy), and entropy were computed as follows:

$$Mean = \frac{1}{N}\sum h\left(i\right) \tag{7}$$

$$CoGx = \frac{1}{\sum h(i)}\sum h\left(i\right)x\left(i\right) \tag{8}$$

$$CoGy = \frac{1}{\sum h(i)}\sum h\left(i\right)y\left(i\right) \tag{9}$$

$$Entropy = -\sum p\left(i\right)log_2 p\left(i\right) \tag{10}$$

where N is the total pixels' value, $h(i)$ is the ith pixel's value in RMS/MDF topographic map, $x\left(i\right)$ is the horizontal coordinate of the ith pixel, $y\left(i\right)$ is the vertical coordinate of the ith pixel, $p(i)$ is the ith pixel's value in RMS/MDF topographic map normalized by the summation of all pixels' values in the map. Entropy is a measure of uniformity of values, which indicates the degree of homogeneity in muscle activation, with higher values corresponding to more uniform distribution of RMS/MDF values over the topographic map [14], [31].

F. Statistical Analysis

SPSS 19.0 (IBM, Armonk, NY, USA) was applied to conduct all statistical analyses. Topographic feature data (RMS_Mean, RMS_CoGx, RMS_CoGy, RMS_Entropy, MDF_Mean, MDF_CoGx, MDF_CoGy, MDF_Entropy) was checked for normality with the Shapiro-Wilk test. A significance level of 0.05 was adopted for all statistical tests, and analyses are performed with topographic feature data match the normality assumption. A one-way repeated measures analysis of variance (ANOVA) was used to compare the difference of topographic feature data between Conditions (NoExo, OffExo, OnExo) in the lifting task. In holding task, we applied a two-way repeated-measures ANOVA, with two within-subject fixed factors (Condition and Phase), to analyze the topographic feature data. Greenhouse-Geisser-corrected significance values were used when the sphericity assumption did not apply. Pairwise multiple comparison post-hoc tests with the least significant difference was conducted for the factor which had a significant main effect according to the ANOVA. Meanwhile, the paired-samples t-test was also applied to compare the difference of data between Phases (First Phase, Second Phase, Third Phase). Partial eta squared (η_p^2) was calculated as a measure of effect size.

IV. Results

A. Analysis of sEMG Topographic Map in the Lifting Task

In the qualitative analysis results depicted in the RMS topographic map and MDF topographic map (Fig. 6), the

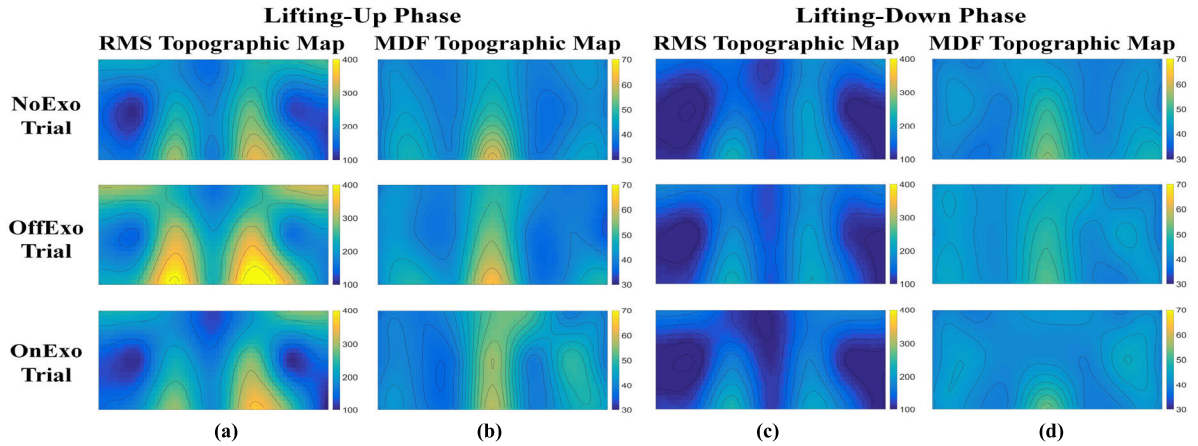

Fig. 6. Comparison of one participant's sEMG topographic map in the lifting task between trials (NoExo trial, OffExo trial, OnExo trial). (a) RMS topographic map at Lifting-Up phase. (b) MDF topographic map at Lifting-Up phase. (c) RMS topographic map at Lifting-Down phase. (d) MDF topographic map at Lifting-Down phase.

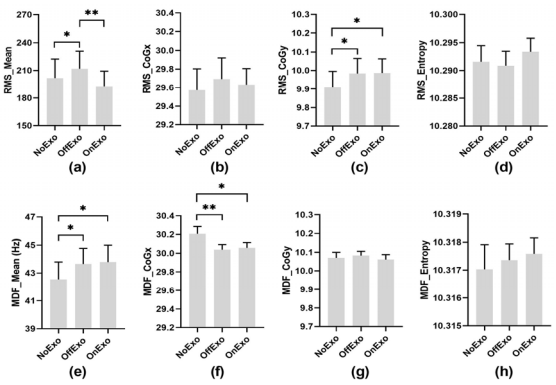

Fig. 7. Comparison of features of sEMG topographic maps in the lifting task between trials at lifting-up phase. (a) Average pixel value over the entire RMS topographic map (RMS_Mean). (b) Coordinate of center of gravity (CoG) of RMS topographic map in the horizontal direction (RMS_CoGx). (c) Coordinate of CoG of RMS topographic map in the vertical direction (RMS_CoGy). (d) Entropy of RMS topographic map (RMS_Entropy). (e) Average pixel value over the entire MDF topographic map (MDF_Mean). (f) Coordinate of CoG of MDF topographic map in the horizontal direction (MDF_CoGx). (g) Coordinate of CoG of MDF topographic map in the vertical direction (MDF_CoGy). (h) Entropy of MDF topographic map (MDF_Entropy). * indicates $p<0.05$. ** indicates $p<0.01$.

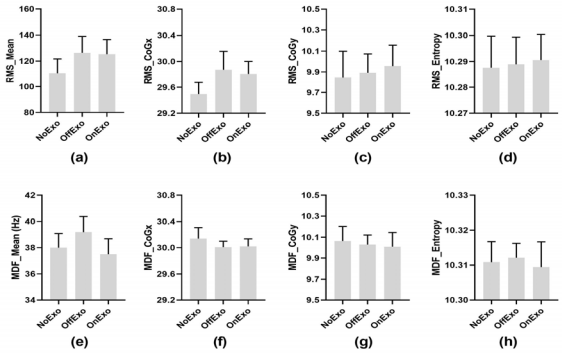

Fig. 8. Comparison of features of sEMG topographic maps in the lifting task between trials at lifting-down phase. (a) RMS_Mean. (b) RMS_CoGx. (c) RMS_CoGy. (d) RMS_Entropy. (e) MDF_Mean. (f) MDF_CoGx. (g) MDF_CoGy. (h) MDF_Entropy. * indicates $p<0.05$. ** indicates $p<0.01$.

high activity region displayed an almost symmetrical distribution from the left side to the right side. This pattern of distribution appeared among NoExo, OffExo, and OnExo trial at both lifting-up and lifting-down phases. The area of the high activity region in the map was different among trials at lifting-up phase. It turned bigger from NoExo to OffExo trial while becoming smaller from OffExo to OnExo trial in RMS topographic map. At lifting-down phase, the map showed no obvious variations.

In quantitative analysis results (Fig. 7, Fig. 8), through one-way repeated measures ANOVA with Condition (NoExo, OffExo, OnExo), there was a statistically significant difference in the RMS_Mean at lifting-up phase, RMS_CoGy at Lifting-Up phase, MDF_Mean at Lifting-Up phase, MDF_CoGx at lifting-up phase. The details were displayed in Table II. Post hoc analysis showed significant difference in the RMS_Mean at lifting-up phase (NoExo vs. OffExo: 201.853±20.593 vs. 211.939±18.990, p=0.040; OffExo vs. OnExo: 211.939±18.990 vs. 192.906±16.451, p=0.003), RMS_CoGy at Lifting-Up phase (NoExo vs. OffExo: 9.908±0.087 vs. 9.984±0.081, p=0.037; NoExo vs. OnExo: 9.908±0.087 vs. 9.987±0.076, p=0.042), MDF_Mean at lifting-up phase (NoExo vs. OffExo: 42.553±1.243 vs. 43.660±1.108, p=0.018; NoExo vs. OnExo: 42.553±1.243 vs. 43.792±1.214, p=0. 033), MDF_CoGx at lifting-up phase (NoExo vs. OffExo: 30.210±0.078 vs. 30.040±0.055, p=0.007; NoExo vs. OnExo: 30.210±0.078 vs. 30.060±0.057, p=0.022). At the lifting-down phase, there was no significant difference among all groups.

B. Analysis of Maintaining Duration in the Holding Task

Through one-way repeated measures ANOVA with Condition (NoExo, OffExo, OnExo), there was a statistically significant difference in maintaining duration [$F(2, 24)=24.868$, $p<0.001$, $\eta_p^2 = 0.675$]. Displayed in Fig. 9, Post hoc analysis showed significant difference between NoExo and OffExo

TABLE II
COMPARISON OF FEATURE PARAMETERS OF sEMG TOPOGRAPHIC MAPS AMONG DIFFERENT EXOSKELETON CONDITIONS IN LIFTING TASK

Movement Phase	Feature Parameter	Condition (NoExo, OffExo, OnExo)		
		Degree of Freedom	η_p^2	P value
Lifting-Up Phase	RMS_Mean	F(2,24)=6.507	0.352	**0.006**
	RMS_CoGx	F(2,24)=0.426	0.034	0.658
	RMS_CoGy	F(2,24)=3.754	0.238	**0.038**
	RMS_Entropy	F(2,24)=1.475	0.109	0.249
	MDF_Mean	F(2,24)=5.199	0.302	**0.013**
	MDF_CoGx	F(2,24)=7.223	0.376	**0.004**
	MDF_CoGy	F(2,24)=1.147	0.087	0.334
	MDF_Entropy	F(1.4,16.8)=0.388	0.031	0.611#
Lifting-Down Phase	RMS_Mean	F(2,24)=3.407	0.221	0.050
	RMS_CoGx	F(2,24)=2.900	0.195	0.074
	RMS_CoGy	F(1.4,16.9)=3.503	0.226	0.067
	RMS_Entropy	F(2,24)=1.857	0.134	0.178
	MDF_Mean	F(1.3,15.4)=2.230	0.157	0.152
	MDF_CoGx	F(2,24)=0.699	0.055	0.507
	MDF_CoGy	F(2,24)=1.109	0.085	0.346
	MDF_Entropy	F(2,24)=1.279	0.096	0.297#

η_p^2 = partial eta squared. RMS = root-mean-square. MDF = median frequency.

# indicates the result has been corrected with the Greenhouse-Geisser measures, because the Mauchly's test of sphericity is not met for the feature parameter.

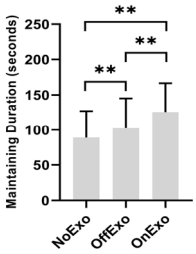

Fig. 9. Comparison of maintaining duration in the holding task between trials (NoExo trial, OffExo trial, OnExo trial). ** indicates p<0.01.

trials (p=0.005), between OffExo and OnExo trial (p=0.001), and between NoExo and OnExo trials (p<0.001).

C. Analysis of sEMG Topographic Map in the Holding Task

Via visually inspection of RMS and MDF topographic maps between trials and within time phases, some particular variation of pattern can be observed (Fig. 10, Fig. 11). On the way from beginning of muscle contraction to fatigue of muscle, all trials (NoExo trial, OffExo trial, OnExo trial) obviously showed increasing area of the high activity region in RMS topographic map and reducing area of the high activity region in MDF topographic map. The similar findings seemed to display for the average pixel value.

The difference between trials in topographic map can also be found (Fig. 10, Fig. 11). In comparison with NoExo and OffExo trials, the OnExo trial significantly showed less variation of area of the high activity region and average pixel value in the topographic map. This finding was also viewed in the change of distribution of high activity region in topographic

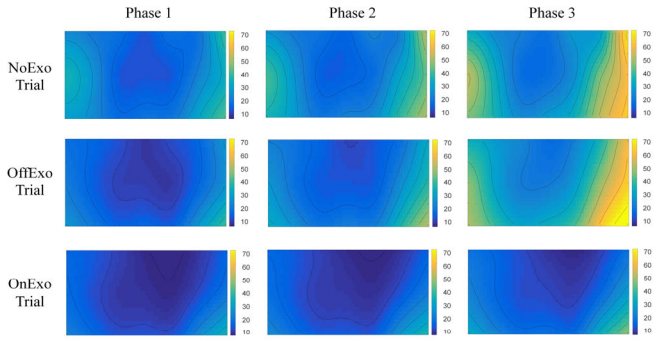

Fig. 10. Comparison of one participant's RMS topographic map in the holding task between trials (NoExo trial, OffExo trial, OnExo trial) and between time phases (First Phase, Second Phase, Third Phase).

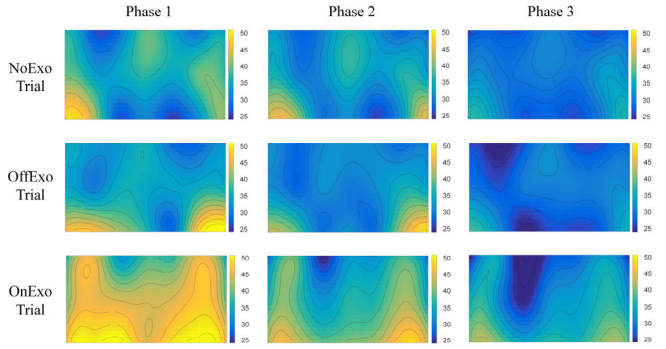

Fig. 11. Comparison of one participant's MDF topographic map in the holding task between trials (NoExo trial, OffExo trial, OnExo trial) and between time phases (First Phase, Second Phase, Third Phase).

map. The symmetry of RMS topographic map in OnExo trial was better and the variation of distribution of high activity region in OnExo trial seemed less.

Through two-way repeated measures ANOVA, all topographic feature parameters showed no Condition × Phase interaction effect. The details were displayed in Table III. The main effects in Condition factor were significantly displayed only for RMS_mean parameter and MDF_mean parameter. For RMS_mean parameter, post-hoc analysis showed significant difference between NoExo and OnExo trials (p=0.009) and between OffExo and OnExo trials (p=0.012). For MDF_mean parameter, post-hoc analysis showed significant difference between NoExo and OnExo trials (p=0.031) and mild significant difference between OffExo and OnExo trials (p=0.054).

The main effects in Phase factor were significantly displayed only for RMS_mean parameter, MDF_mean parameter, MDF_CoGy parameter, and MDF_Entropy parameter. For RMS_mean parameter, post-hoc analysis showed significant difference between the first phase and the third phase (p=0.032) and between the second phase and the third phase (p=0.012). For MDF_mean parameter, post-hoc analysis showed significant difference between the first phase and the second phase (p=0.016), between the first phase and the third phase (p=0.006) and between the second phase and the third phase (p=0.014). For MDF_CoGy parameter, post-hoc analysis showed significant difference between the first phase and the third phase (p=0.008) and between the second phase and the third phase (p=0.001). For MDF_Entropy

TABLE III
COMPARISON OF FEATURE PARAMETERS OF SEMG TOPOGRAPHIC MAPS AMONG DIFFERENT EXOSKELETON CONDITIONS AND TIME PHASES IN HOLDING TASK

Feature Parameter	Condition			Phase			Condition × Phase		
	Degree of Freedom	η_p^2	P value	Degree of Freedom	η_p^2	P value	Degree of Freedom	η_p^2	P value
RMS_Mean	F(2,24) =6.012	0.334	**0.008**	F(1.02,12.29) =6.065	0.336	**0.029#**	F(2.69,32.27) =2.731	0.185	0.065#
RMS_CoGx	F(1.19,14.28) =0.030	0.003	0.900#	F(1.35,16.14) =1.629	0.120	0.225#	F(4,48) =0.052	0.004	0.995
RMS_CoGy	F(2,24) =0.744	0.058	0.486	F(1.15,13.79) =1.574	0.116	0.234#	F(2.51,30.10) =0.515	0.041	0.643#
RMS_Entropy	F(2,24) =0.912	0.071	0.415	F(1.35,16.22) =1.112	0.085	0.329#	F(1.78,21.38) =0.185	0.015	0.808#
MDF_Mean	F(2,24) =3.844	0.243	**0.036**	F(1.24,14.87) =9.887	0.452	**0.005#**	F(1.96,23.55) =0.152	0.012	0.856#
MDF_CoGx	F(1.38,16.59) =1.772	0.129	0.203#	F(2,24) =2.131	0.151	0.141	F(4,48) =0.473	0.038	0.756
MDF_CoGy	F(2,24) =0.710	0.056	0.502	F(1.35,16.18) =9.212	0.434	**0.005#**	F(2.35,28.18) =0.028	0.002	0.984#
MDF_Entropy	F(1.38,16.54) =0.384	0.031	0.611#	F(2,24) =19.272	0.616	**<0.001**	F(2.46,29.49) =1.048	0.080	0.375#

η_p^2 = partial eta squared. RMS = root-mean-square. MDF = median frequency.
# indicates the result has been corrected with the Greenhouse-Geisser measures, because the Mauchly's test of sphericity is not met for the feature parameter.

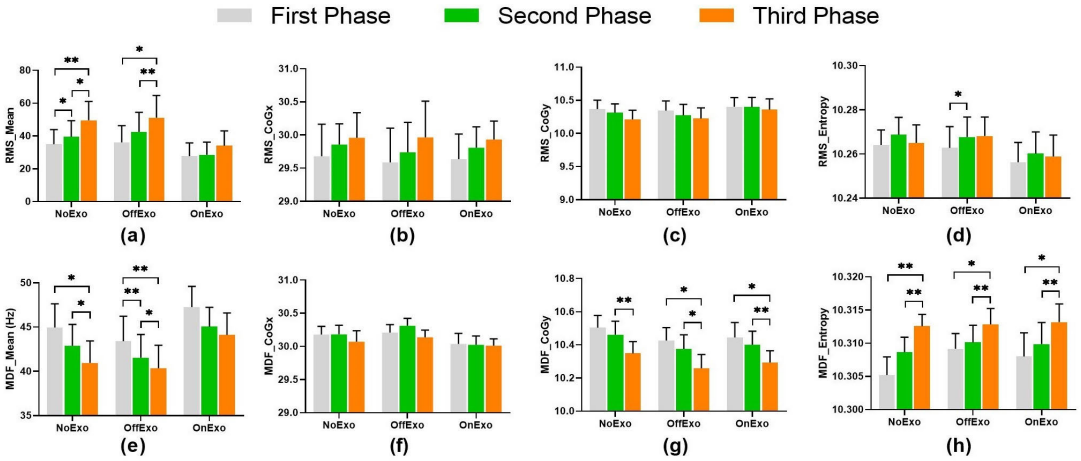

Fig. 12. Comparison of features of sEMG topographic maps in the holding task between trials. (a) Average pixel value over the entire RMS topographic map (RMS_Mean). (b) Coordinate of center of gravity (CoG) of RMS topographic map in the horizontal direction (RMS_CoGx). (c) Coordinate of CoG of RMS topographic map in the vertical direction (RMS_CoGy). (d) Entropy of RMS topographic map (RMS_Entropy). (e) Average pixel value over the entire MDF topographic map (MDF_Mean). (f) Coordinate of CoG of MDF topographic map in the horizontal direction (MDF_CoGx). (g) Coordinate of CoG of MDF topographic map in the vertical direction (MDF_CoGy). (h) Entropy of MDF topographic map (MDF_Entropy). * indicates $p<0.05$. ** indicates $p<0.01$.

parameter, post-hoc analysis showed significant difference between the first phase and the second phase ($p=0.026$), between the first phase and the third phase ($p<0.001$) and between the second phase and the third phase ($p<0.001$). The comparison of features of sEMG topographic maps in the holding task between trials through paired-samples t-test was also displayed in the Fig. 12.

V. DISCUSSION

This study tried to apply sEMG topographic map to investigate the effect of lumbar exoskeleton on the coordinated activities of low back muscles. During lifting-up phase of the lifting task, the average pixel values of RMS and MDF maps for the NoExo trial were significantly lower than those for the OffExo trial, but were not significantly higher than those for the OnExo trial. The distribution of CoG showed a significant difference between NoExo and OffExo/OnExo trials. In the holding task, the average pixel values of RMS and MDF maps showed significant differences between NoExo/OffExo and OnExo trials. The effect sizes (η_p^2) for all parameter variables, which exhibited a statistically significant difference ($p<0.05$), were larger than 0.1379. According to the previous commonly-cited study on effect size [32], it indicated the relevance of the difference can be considered substantial. Thus,

people wearing the active lumbar exoskeleton are able to reduce the load, which was from both the exoskeleton and lifted box, on their low back muscles in the static holding task rather than in the dynamic lifting task.

A. RMS and MDF in the Tasks

The muscle activation depends on the number of recruited motor units (MUs) and the firing rate of those MUs [33]. They can be partially expressed by the RMS and MDF parameters extracted from the sEMG signal [34]. In this study, in the lifting task, the average RMS pixel values of the sEMG topographic map increased when the subjects wore the unpowered lumbar exoskeleton. It significantly and simultaneously reduced while the exoskeleton started to work. It indicated, during isotonic muscle contraction, although the loading of the powered lumbar exoskeleton could reduce the muscle activation, loading of the unpowered lumbar exoskeleton increased it. It seemed the weight attached to the low back muscles was larger than the reduced activation of low back muscles caused by the unpowered lumbar exoskeleton. When loading the powered lumbar exoskeleton, the average RMS pixel values were significantly reduced but still showed no significant difference with those without any lumbar exoskeleton. Thus, in order to relieve the physical workload in the lifting task, the weight of the lumbar exoskeleton should be decreased as much as possible. This finding coincides with those in the previous studies on upper-limb and lower-limb exoskeletons [35], [36], [37].

In the holding task, muscle fatigue can be indicated by the MDF parameter from sEMG signal, which shows high correlation with the conduction velocity (CV) of motor unit action potential (MUAP) [38], [39]. In this study, generally for all trials, the average RMS pixel value of sEMG topographic map increased as the muscle fatigue became more and more severe while the average MDF pixel value decreased. It is similar with previous findings that fatigue reliably produces a decrease of the frequency feature of sEMG and increase of amplitude feature of sEMG for some specific muscles during static contraction [40], [41]. It indicated the fatigue-related changes in myoelectric properties involved a decrease of muscle CV [42], [43]. Different with the findings in the lifting task, the repeated measures ANOVA showed the change trend of average RMS and MDF pixel values did not show significant difference between NoExo and OffExo trials in the holding task, while they significantly varied in the OnExo trial. It implied that, by wearing a powered lumbar exoskeleton, the number of recruited MUs, the firing rate of those MUs and the global CV of MUAP showed no significant variation with the increasing fatigue. This finding is almost consistent with the result of fatigue-related characteristics (maintaining duration of holding posture: NoExo/OffExo vs. OnExo, $p<0.05$). It indicated, compared with the muscles from the legs and arms, low back muscles can be better kept from fatigue by using the powered lumbar exoskeleton in the holding task. In addition, the maintaining duration between NoExo and OffExo group also showed a significant difference. It might be because the exoskeleton without power can still give some assistance, which seemed to be not given to the low back muscles, through the biomechanical structure.

B. Center of Gravity in the Tasks

The spatial distribution of CoG in sEMG topographic map were different in the lifting task and the holding task. In the holding task, time-related change of position of CoG in the RMS and MDF topographic maps showed no significant difference among NoExo, OffExo and OnExo trials. In the lifting task, both the vertical coordinate value of CoG (CoGy) in the RMS topographic map and the horizonal coordinate value of CoG (CoGx) in the MDF topographic map significantly moved closer to the center of the map from trial without exoskeleton to trial with exoskeleton. It indicated the activation and coordination of some superficial back and hip muscle groups (the entire erector spinae, part of latissimus dorsi, and part of gluteus maximus) [44] were different in the two tasks when wearing the lumbar exoskeleton. Specifically, the erector spinae played a larger role while wearing the lumbar exoskeleton in the lifting task because the vertical coordinate value of CoG in the RMS topographic map moved downward. The gravity towards the earth's center may account for the cause of this finding [45]. When subjects flexed and extended their lumbar spine, the weight of the lumbar exoskeleton transferred in gravity's direction so that the erector spinae supported most of the weight. In addition, the activation of the back and hip muscles between the left side and right side of the spine was more symmetrical after the subject wore the lumbar exoskeleton. It may be due to the applied weight of the exoskeleton. However, these findings were not observed in the holding task, which indicated the exoskeleton cannot affect the distribution of muscle activity under the fatigue state.

C. Entropy in the Tasks

Entropy can be used to measure the uniformity of values [14]. In this study, only the entropy of the RMS topographic map in the fatigue-related holding task showed a difference between trials. However, the ANOVA test did not show a significant main effect in Conditions. Because the entropy provides an estimation of homogeneity between signals of the whole 2D EMG map [46], [47], the findings of this study indicated that the changing pattern of the heterogeneity of the distribution of low back muscle activities would not be affected by wearing the powered lumbar exoskeleton.

D. Advantage of sEMG Topographic Map

The sEMG topographic map used in this study was constructed based on the multi-channel array's sEMG technique. Unlike the HD-sEMG technique, it has no requirement for the inter-electrode distance and the electrode size [28], [29]. This advantage was significant while comparing the sEMG topographic maps among different subjects. It was because the sEMG topographic maps were asked to be anatomically consistent for all subjects. To meet this requirement, the multi-channel sEMG technique was preferred due to its even placement of the multi-channel electrodes across the entire low back region. Additionally, the relatively large size of the

multi-channel electrodes reduced the risk of detachment from the skin during trunk movements while wearing the lumbar exoskeleton. Consequently, the sEMG topographic map can be accurately and reliably generated from high-quality sEMG signals.

E. Limitations

There are several limitations in this study. Firstly, although the sample size of this study is enough to reach a conclusion, the conclusion can be more convincing by recruiting more subjects. In the current study, all recruited participants were male and young. The diversity of the recruited subjects should be increased in the future. Secondly, more lumbar movements should be conducted. The lumbar movement in this study was designed as a simple lift-drop movement (stoop lifting), in order to obtain a preliminary finding about the usefulness of sEMG topographic map. In the daily work and life, the lumbar movement is not limited to the stoop lifting. It also includes squat lifting, lifting with rotation, and so forth [48]. The lumbar sEMG topographic map during these lumbar movements should be explored in the future. Thirdly, additional measurements of the low back muscles (e.g., muscle force, muscle thickness, muscle electrical impedance) should be explored in future studies [49], [50], [51], since there was no observed difference in muscle activation with and without a powered exoskeleton. Finally, the muscle fatigue state in this study is activated only in the holding task. Because the development of muscle fatigue depends upon the mode of muscle contraction (static isometric contraction or dynamic isotonic contraction) [52], it is meaningful to compare the difference in coordinated activities of low back muscles under different types of muscle fatigue states when wearing lumber exoskeleton. Future investigations should be conducted.

VI. Conclusion

Using sEMG topographic maps, this study finds that the active lumbar exoskeleton can reduce the load on low back muscles in the static holding task rather than in the dynamic lifting task. It is proved that sEMG topographic mapping offers a new method to evaluate the effect of lumbar exoskeletons on coordinated activities of low back muscles more deeply, thereby helping improve the design of lumbar exoskeleton systems.

References

[1] C. DeRosa and J. A. Porterfield, "Anatomical linkages and muscle slings of the lumbopelvic region," in *Movement, Stability & Lumbopelvic Pain*, 2nd ed., A. Vleeming, V. Mooney, R. Stoeckart, and P. Wilson, Eds. Edinburgh, Scotland: Churchill Livingstone, 2007, ch. 2, pp. 47–62.

[2] R. Buchbinder et al., "Low back pain: A call for action," *Lancet*, vol. 391, no. 10137, pp. 2384–2388, Aug. 2018.

[3] X. Ji, D. Wang, P. Li, L. Zheng, J. Sun, and X. Wu, "SIAT-WEXv2: A wearable exoskeleton for reducing lumbar load during lifting tasks," *Complexity*, vol. 2020, Nov. 2020, Art. no. 8849427.

[4] E. B. Weston, M. Alizadeh, G. G. Knapik, X. Wang, and W. S. Marras, "Biomechanical evaluation of exoskeleton use on loading of the lumbar spine," *Appl. Ergonom.*, vol. 68, pp. 101–108, Apr. 2018.

[5] K. Miura et al., "The hybrid assisted limb (HAL) for care support, a motion assisting robot providing exoskeletal lumbar support, can potentially reduce lumbar load in repetitive snow-shoveling movements," *J. Clin. Neurosci.*, vol. 49, pp. 83–86, Mar. 2018.

[6] S. Iranzo et al., "Assessment of a passive lumbar exoskeleton in material manual handling tasks under laboratory conditions," *Sensors*, vol. 22, no. 11, p. 4060, May 2022.

[7] X. Yong, Z. Yan, C. Wang, C. Wang, N. Li, and X. Wu, "Ergonomic mechanical design and assessment of a Waist assist exoskeleton for reducing lumbar loads during lifting task," *Micromachines*, vol. 10, no. 7, p. 463, Jul. 2019.

[8] J. Li et al., "Development and evaluation of a lumbar assisted exoskeleton with mixed lifting tasks by various postures," *IEEE Trans. Neural Syst. Rehabil. Eng.*, vol. 31, pp. 2111–2119, 2023.

[9] O. Thamsuwan, S. Milosavljevic, D. Srinivasan, and C. Trask, "Potential exoskeleton uses for reducing low back muscular activity during farm tasks," *Amer. J. Ind. Med.*, vol. 63, no. 11, pp. 1017–1028, Nov. 2020.

[10] C. K. Tan et al., "Muscle synergies during repetitive stoop lifting with a bioelectrically-controlled lumbar support exoskeleton," *Frontiers Hum. Neurosci.*, vol. 13, p. 142, Apr. 2019.

[11] M. J. Escalona, D. Bourbonnais, D. Le Flem, M. Goyette, C. Duclos, and D. H. Gagnon, "Effects of robotic exoskeleton control options on lower limb muscle synergies during overground walking: An exploratory study among able-bodied adults," *Neurophysiol. Clinique*, vol. 50, no. 6, pp. 495–505, Nov. 2020.

[12] C. L. Banks, M. M. Pai, T. E. McGuirk, B. J. Fregly, and C. Patten, "Methodological choices in muscle synergy analysis impact differentiation of physiological characteristics following stroke," *Frontiers Comput. Neurosci.*, vol. 11, pp. 1–12, Aug. 2017.

[13] K. M. Steele, M. C. Tresch, and E. J. Perreault, "Consequences of biomechanically constrained tasks in the design and interpretation of synergy analyses," *J. Neurophysiol.*, vol. 113, no. 7, pp. 2102–2113, Apr. 2015.

[14] D. Farina, F. Leclerc, L. Arendt-Nielsen, O. Buttelli, and P. Madeleine, "The change in spatial distribution of upper trapezius muscle activity is correlated to contraction duration," *J. Electromyogr. Kinesiol.*, vol. 18, no. 1, pp. 16–25, Feb. 2008.

[15] F. V. dos Anjos, M. Ghislieri, G. L. Cerone, T. P. Pinto, and M. Gazzoni, "Changes in the distribution of muscle activity when using a passive trunk exoskeleton depend on the type of working task: A high-density surface EMG study," *J. Biomechanics*, vol. 130, Jan. 2022, Art. no. 110846.

[16] E. Martinez-Valdes et al., "Consensus for experimental design in electromyography (CEDE) project: Single motor unit matrix," *J. Electromyogr. Kinesiol.*, vol. 68, Feb. 2023, Art. no. 102726.

[17] K. K. Y. Leung et al., "High-density surface electromyography for swallowing evaluation in post-radiation dysphagia," *Laryngoscope*, vol. 133, no. 11, pp. 2920–2928, Nov. 2023.

[18] N. Habibzadeh, "Physiology of distinct modes of muscular contraction," *Int. Physiol. J.*, vol. 1, no. 3, pp. 1–8, Oct. 2018.

[19] J. Kallio, K. Søgaard, J. Avela, P. V. Komi, H. Selänne, and V. Linnamo, "Motor unit firing behaviour of soleus muscle in isometric and dynamic contractions," *PLoS ONE*, vol. 8, no. 2, Feb. 2013, Art. no. e53425.

[20] J. R. Moldover and J. Borg-Stein, "Exercise and fatigue," in *The Physiological Basis of Rehabilitation Medicine*, J. A. Downey, S. J. Myers, E. G. Gonzalez, and J. S. Lieberman, Eds., 2nd ed. Oxford, U.K.: Butterworth-Heinemann, 1994, ch. 15, pp. 393–411.

[21] S. Toxiri, J. Ortiz, J. Masood, J. Fernández, L. A. Mateos, and D. G. Caldwell, "A wearable device for reducing spinal loads during lifting tasks: Biomechanics and design concepts," in *Proc. IEEE Int. Conf. Robot. Biomimetics (ROBIO)*, Dec. 2015, pp. 2295–2300.

[22] S. Toxiri et al., "Rationale, implementation and evaluation of assistive strategies for an active back-support exoskeleton," *Frontiers Robot. AI*, vol. 5, p. 53, May 2018.

[23] D. J. Hyun, H. Lim, S. Park, and S. Nam, "Singular wire-driven series elastic actuation with force control for a Waist assistive exoskeleton, H-WEXv2," *IEEE/ASME Trans. Mechatronics*, vol. 25, no. 2, pp. 1026–1035, Apr. 2020.

[24] T. Sa-ngiamsak, N. Phatrabuddha, T. Yingratanasuk, and A. Thetkathuek, "Long-haul logistic truck drivers' physiological fatigue on low back and shoulder: A primary exploration," in *Occupational and Environmental Safety and Health II*, P. Arezes et al., Ed. Cham, Switzerland: Springer, 2020, pp. 367–375.

[25] E. F. Maughan and J. S. Lewis, "Outcome measures in chronic low back pain," *Eur. Spine J.*, vol. 19, no. 9, pp. 1484–1494, Sep. 2010.

[26] M. Fischer and S. S. Schäfer, "Effects of changes in pH on the afferent impulse activity of isolated cat muscle spindles," *Brain Res.*, vol. 1043, nos. 1–2, pp. 163–178, May 2005.

[27] H. Jebelli and S. Lee, "Feasibility of wearable electromyography (EMG) to assess construction workers' muscle fatigue," in *Advances in Informatics and Computing in Civil and Construction Engineering*. Cham, Switzerland: Springer, 2019, pp. 181–187.

[28] N. Jiang, J. Wei, G. Li, B. Wei, F. F. Zhu, and Y. Hu, "Effect of dry-electrode-based transcranial direct current stimulation on chronic low back pain and low back muscle activities: A double-blind sham-controlled study," *Restorative Neurol. Neurosci.*, vol. 38, no. 1, pp. 41–54, Feb. 2020.

[29] N. Jiang, K. D.-K. Luk, and Y. Hu, "A machine learning-based surface electromyography topography evaluation for prognostic prediction of functional restoration rehabilitation in chronic low back pain," *Spine*, vol. 42, no. 21, pp. 1635–1642, Nov. 2017.

[30] M. Rojas-Martínez, M. A. Mañanas, J. F. Alonso, and R. Merletti, "Identification of isometric contractions based on high density EMG maps," *J. Electromyogr. Kinesiol.*, vol. 23, no. 1, pp. 33–42, Feb. 2013.

[31] L. Li, X. Wang, B. Yao, X. Zhang, and P. Zhou, "Sample entropy-based surface electromyographic examination with a linear electrode array in survivors with spinal cord injury," *IEEE Trans. Neural Syst. Rehabil. Eng.*, vol. 31, pp. 2944–2952, 2023.

[32] J. Cohen, *Statistical Power Analysis for the Behavioral Sciences*, 2nd ed. New York, NY, USA: Lawrence Erlbaum Associates, 1988.

[33] Z. Erim, C. J. De Luca, K. Mineo, and T. Aoki, "Rank-ordered regulation of motor units," *Muscle Nerve*, vol. 19, no. 5, pp. 563–573, May 1996.

[34] C. Orizio, M. Solomonow, R. Baratta, and A. Veicsteinas, "Influence of motor units recruitment and firing rate on the soundmyogram and EMG characteristics in cat gastrocnemius," *J. Electromyogr. Kinesiol.*, vol. 2, no. 4, pp. 232–241, Jan. 1992.

[35] X. Jin, Y. Cai, A. Prado, and S. K. Agrawal, "Effects of exoskeleton weight and inertia on human walking," in *Proc. IEEE Int. Conf. Robot. Autom. (ICRA)*, May 2017, pp. 1772–1777.

[36] S. S. Kawale and M. Sreekumar, "Design of a wearable lower body exoskeleton mechanism for shipbuilding industry," *Proc. Comput. Sci.*, vol. 133, pp. 1021–1028, Jan. 2018.

[37] A. S. Gorgey, "Robotic exoskeletons: The current pros and cons," *World J. Orthopedics*, vol. 9, no. 9, pp. 112–119, Sep. 2018.

[38] R. Merletti, M. Knaflitz, and C. J. De Luca, "Myoelectric manifestations of fatigue in voluntary and electrically elicited contractions," *J. Appl. Physiol.*, vol. 69, no. 5, pp. 1810–1820, Nov. 1990.

[39] D. Farina, M. Fosci, and R. Merletti, "Motor unit recruitment strategies investigated by surface EMG variables," *J. Appl. Physiol.*, vol. 92, no. 1, pp. 235–247, Jan. 2002.

[40] B. Gerdle, B. Larsson, and S. Karlsson, "Criterion validation of surface EMG variables as fatigue indicators using peak torque: A study of repetitive maximum isokinetic knee extensions," *J. Electromyogr. Kinesiol.*, vol. 10, no. 4, pp. 225–232, Aug. 2000.

[41] P. A. Ortega-Auriol, T. F. Besier, W. D. Byblow, and A. J. C. Mcmorland, "Fatigue influences the recruitment, but not structure, of muscle synergies," *Frontiers Hum. Neurosci.*, vol. 12, p. 217, Jun. 2018.

[42] R. M. Enoka and J. Duchateau, "Muscle fatigue: What, why and how it influences muscle function," *J. Physiol.*, vol. 586, no. 1, pp. 11–23, Jan. 2008.

[43] J. L. Dideriksen, R. M. Enoka, and D. Farina, "Neuromuscular adjustments that constrain submaximal EMG amplitude at task failure of sustained isometric contractions," *J. Appl. Physiol.*, vol. 111, no. 2, pp. 485–494, Aug. 2011.

[44] M. Balasch-Bernat, T. Willems, L. Danneels, M. Meeus, and D. Goubert, "Differences in myoelectric activity of the lumbar muscles between recurrent and chronic low back pain: A cross-sectional study," *BMC Musculoskeletal Disorders*, vol. 22, no. 1, p. 756, Sep. 2021.

[45] E. Verlinde, "On the origin of gravity and the laws of Newton," *J. High Energy Phys.*, vol. 2011, no. 4, p. 29, Apr. 2011.

[46] E. Martinez-Valdes, F. Wilson, N. Fleming, S.-J. McDonnell, A. Horgan, and D. Falla, "Rowers with a recent history of low back pain engage different regions of the lumbar erector spinae during rowing," *J. Sci. Med. Sport*, vol. 22, no. 11, pp. 1206–1212, Nov. 2019.

[47] A. Sanderson et al., "People with low back pain display a different distribution of erector spinae activity during a singular monoplanar lifting task," *Frontiers Sports Act. Living*, vol. 1, p. 65, Dec. 2019.

[48] Ž. Kozinc, J. Babič, and N. Šarabon, "Comparison of subjective responses of low back pain patients and asymptomatic controls to use of spinal exoskeleton during simple load lifting tasks: A pilot study," *Int. J. Environ. Res. Public Health*, vol. 18, no. 1, p. 161, Dec. 2020.

[49] P. Schenk, A. Klipstein, S. Spillmann, J. Strøyer, and T. Laubli, "The role of back muscle endurance, maximum force, balance and trunk rotation control regarding lifting capacity," *Eur. J. Appl. Physiol.*, vol. 96, no. 2, pp. 146–156, Jan. 2006.

[50] L. Ge et al., "Effects of core stability training on older women with low back pain: A randomized controlled trial," *Eur. Rev. Aging Phys. Activity*, vol. 19, no. 1, p. 10, Apr. 2022.

[51] H. Wang et al., "Electrical properties of lumbar paraspinal muscles in young adults with and without chronic low back pain based on electrical impedance myography: A cross-sectional study," *Frontiers Neurol.*, vol. 12, Feb. 2022, Art. no. 789589.

[52] P. Vedsted, A. H. Larsen, K. Madsen, and G. Sjøgaard, "Muscle performance following fatigue induced by isotonic and quasi-isometric contractions of rat extensor digitorum longus and soleus muscles in vitro," *Acta Physiol. Scandinavica*, vol. 178, no. 2, pp. 86–175, Jun. 2003.